JOURNAL OF COMPUTATIONAL PHYSICS 111, 381–389 (1994)

Finite Volume TVD Scheme on an Unstructured Grid System for Three-Dimensional MHD Simulation of Inhomogeneous Systems Including Strong Background Potential Fields

T. TANAKA

Communication Research Laboratory, Koganei-shi, Tokyo 184, Japan

Received December 23, 1992; revised June 29, 1993

A three-dimensional (3D) high-resolution MHD simulation scheme on an unstructured grid system is developed for inhomogeneous systems, including strong background potential fields. The scheme is based on the finite volume method (FVM) with an upwinding numerical flux by the linearized Riemann solver. Upwindings on an unstructured grid system are realized from the fact that the MHD equations are symmetric with the rotation of the space. The equation system is modified to avoid direct inclusions of the background potential field as a dependent variable, through the use of changed dependent variables. Despite such a change of the equation system, the eigenvectors in the mode-synthesis matrix that are necessary for the evaluation of the upwinding numerical flux vectors can still be written analytically. The eigenvalues of the MHD flux Jacobian matrix that are also necessary for the upwinding calculations are derived from the well-known Alfven, fast and slow, velocities. The calculations of the eigen vectors is done with special care when the wave propagations become parallel or perpendicular to the ambient magnetic field, because degeneration of the eigenvalues occurs in these cases. To obtain a higher order of accuracy, the upwinding flux is extended to the second-order TVD numerical flux in the calculation of FVM, through the MUSCL approach and Van Leer's differentiable limiter. In order to show the efficiency of the above scheme, a numerical example is given for the interaction process of high-β supersonic plasma flow with the region of a strong dipole field, including magnetized low-β plasma.

1. INTRODUCTION

In recent years, magneto-hydrodynamic (MHD) simulation has attained an important position in the studies of space and astrophysical problems [1–5]. Works in these studies have gone in the direction of three-dimensional (3D) MHD calculations, since the problems are inherently three-dimensional. A serious difficulty in numerical MHD calculations when applied to space and astrophysics comes from the fact that many problems include strong non-uniformities in treating various regions. Although there are many previous works applying MHD simulation to space and astrophysics, much effort is still needed to extend the application of MHD simulation to problems which include strong non-uniformities.

In the area of hydrodynamical calculations, on the other hand, much effort has been devoted in recent years, to constructing efficient finite difference schemes, extending upwind schemes to a higher order of accuracy [6]. Among the many upwind schemes, very popular schemes are: (1) based on the Roe's approximate linearized Riemann solver, (2) based on non-linear approximations of systems such as Godunov or Osher [7], and (3) based on flux splittings by Steger and Warming or by Van Leer. As higher order extensions of upwind schemes, several types of high-resolution schemes are currently in use. These include total variation diminishing schemes are currently in use. These include total variation diminishing (TVD), total variation bounded (TVB), and essentially non-oscillatory (ENO) finite difference schemes [6, 8].

The notion of TVD was first introduced by Harten [8]. He derived a set of sufficient conditions useful to construct second-order TVD schemes. The mechanism that is widely used for satisfying the TVD condition involves some kind of limiting procedures. Adopting TVD finite difference schemes, one can obtain sharper profiles to represent discontinuities, whilst avoiding spurious oscillations.

There are many approaches to construct TVD schemes from upwind schemes. Higher-order TVD schemes are constructed using MUSCL or non-MUSCL approaches [9]. The MUSCL approach is efficient to construct TVD schemes from Roe's scheme or flux split schemes. On the other hand, the non-MUSCL approach for TVD schemes can be used, employing an approximate linearized Riemann solver, and is divided into two types: symmetric TVD and upwind TVD schemes.

The concept of TVD conditions can be extended to MHD equations. If an upwind MHD numerical scheme satisfies the TVD condition, it enables a stable computation with high resolution and effective shock capturing. Brio and Wu [10] showed a method to construct an upwind scheme for one-dimentional MHD equations. Because the method of flux splitting for MHD equations is not known at the

0021-9991/94 $6.00

present time, Brio and Wu [10] constructed an upwind finite difference scheme for MHD equations adopting Roe's linearization procedure. Brio and Wu [10] also concluded that non-linear upwind methods are too involved for MHD equations.

Tanaka [11] extended the work of Brio and Wu [10] to 3D calculations, aiming at the application of MHD equations to space and astrophysical problems. In order to overcome difficulties in numerical calculations caused by spatial non-uniformities, which are generally included in space and astrophysical problems, Tanaka [11] developed an upwinding MHD scheme on unstructured grid systems. The framework employed for MHD simulations on unstructured grid systems is the finite volume method (FVM), based on the conservation law [12]. Upwindings in FVM are achieved by adopting an important property of MHD equations that their forms are symmetric with the rotation of the space. In this framework, numerical integrations of hyperbolic MHD equations can be stabilized through the use of the TVD numerical flux based on the MUSCL approach with the linearized Riemann solver.

The phenomenon controlled by the coupling process between different regions having quite different characteristics seems to be more difficult to treat numerically. For example, auroral physics is a typical case. In interplanetary space, the earth's magnetic field and plasma environment interact with the solar wind which is the inevitable result of the steady outflow of the ionized solar atmosphere. As a result, the magnetospheric region is formed around the Earth and energy flows in from the solar wind to the magnetosphere. The auroral breakup is the release of this energy from the magnetosphere to the polar ionosphere, which is situated at the lower altitude near the Earth, interchanging the field-aligned currents (FAI) between the two regions [13, 14]. In this problem, therefore, the main process to be studied is the coupling effects between the two different regions, namely the magnetosphere and the ionosphere [15].

The representative sizes of the magnetosphere and the ionosphere are extremely different. In order to calculate the complex distributions of the ionospheric currents associated with auroral phenomena, the grid spacing must be less than 100 km. On the other hand, the size of the magnetosphere exceeds more than 100,000 km. If one uses a Cartesian coordinate system and covers all of the magnetospheric and ionospheric regions by a grid system which is sufficient for the analysis of ionospheric phenomena, the total number of grid points will far exceed the available size of computer memory. However, the number of grid points for the magnetospheric region can be reduced to a large extent because the characteristic scale of magnetospheric dynamics is much larger than that of the ionosphere. In order to achieve such a reduction of grid points, it is necessary to use different grid point densities according to respective regions. This reduction of grid points becomes more and more effective when the study goes to higher dimensions. Of course, the computational time is reduced in proportion to the reduction of grid points.

In many cases, planets and stars have a strong magnetic field generated in their interior regions. In the case of the Earth, the magnitude of the dipole magnetic field is about 30,000 nT in the ionospheric region near the Earth, while it diminishes rapidly in the magnetosphere to about 10 nT. Therefore, the magnitude of the intrinsic magnetic field varies over a wide range in treating the whole region in the problem of magnetosphere–ionosphere coupling. On the other hand, the variable components of the magnetic field, which are calculated from MHD equations, exhibit a similar magnitude over the whole region. As a result, the ratio of variable to intrinsic components of the magnetic field becomes extremely small in the ionospheric region. These situations give other difficulties in the numerical study of the coupling process between two different regions. Especially, severe difficulties appear in the energy equation. However, this difficulty, due to the wide range in the ratio of variable to internal magnetic fields, can be avoided due to the fact that the intrinsic magnetic field includes only potential components. Thus, it becomes important to construct MHD calculations that suppress the direct inclusion of the intrinsic components of the magnetic field as dependent variables. In this paper, therefore, a modified equation system will be derived considering such intention through a change in the dependent variables. It will be shown that an equation system with the above modification can be written in the conservation form and can still be treated numerically through the upwinding TVD flux.

There are many other problems in space and astrophysics which require the simultaneous treatment of several regions having quite different characteristics. For the study of problems hitherto mentioned by numerical MHD simulation, the requirements are increasing for the use of a non-uniform grid system and the suppression of the potential-field calculations as dependent variables. To achieve a flexible grid distribution in 3D space aiming at an application to the problems which include strong non-uniformities, unstructured grid systems are more suited than structured grid systems. Unstructured grid systems are also suited for the construction of a 3D body-fit grid system around the Earth, the sun, and stars, which are the main objects of space and astrophysical studies.

Now it becomes the purpose of this paper to develop a new MHD numerical scheme which satisfies the following conditions, aiming at the application to space and astrophysical problems; it is: (1) applicable to systems with strong non-uniformities caused by an inhomogeneous background potential field; (2) available on 3D unstructured grid systems; and (3) in the form of a TVD scheme with a higher order of accuracy.

2. BASIC EQUATIONS

The non-dimensional conservation-law form of the ideal MHD equations can be written in the Cartesian coordinate system (x, y, z, t) as

$$\frac{\partial \mathbf{u}}{\partial t}+\frac{\partial \mathbf{F}}{\partial x}+\frac{\partial \mathbf{G}}{\partial y}+\frac{\partial \mathbf{H}}{\partial z}=0, \tag{1}$$

where the dependent variables are $\mathbf{u}=(\rho, m_x, m_y, m_z, B_x, B_y, B_z, U)^{\mathrm{T}}$, and $\mathbf{F}$, $\mathbf{G}$, and $\mathbf{H}$ are flux functions in the x, y, and z directions, ρ is the density, $\mathbf{m}$ is the momentum, $\mathbf{B}$ is the magnetic field, and U is the energy density. Using Gauss's law, the integration form of Eq. (1) can be written as

$$\frac{\partial}{\partial t}\int \mathbf{u}\, dv+\int (\mathbf{F}n_x+\mathbf{G}n_y+\mathbf{H}n_z)\, ds=0, \tag{2}$$

where dv and ds are the volume and surface elements of the control volume and $\mathbf{n}$ is a unit vector normal to the surface of the control volume.

Let us define a matrix which rotates the x axis to the direction of $\mathbf{n}$

$$T=\begin{vmatrix} 1 & & & 0 \\ & T_1 & & \\ & & T_1 & \\ 0 & & & 1 \end{vmatrix}, \tag{3}$$

with

$$T_1=\begin{vmatrix} n_x & n_y & n_z \\ t_{1x} & t_{1y} & t_{1z} \\ t_{2x} & t_{2y} & t_{2z} \end{vmatrix}, \tag{4}$$

then Eq. (2) is expressed as

$$\frac{\partial}{\partial t}\int \mathbf{u}\, dv+\int T^{-1}T(\mathbf{F}n_x+\mathbf{G}n_y+\mathbf{H}n_z)\, ds=0, \tag{5}$$

where $\mathbf{t}_1$ and $\mathbf{t}_2$ are unit vectors tangential to the surface of the control volume and orthogonal to each other. Since the form of the MHD equations must be unchanged for the rotation of the coordinate system, the relation

$$T(\mathbf{F}(\mathbf{u})\, n_x+\mathbf{G}(\mathbf{u})\, n_y+\mathbf{H}(\mathbf{u})\, n_z)=\mathbf{F}(T\mathbf{u})=\mathbf{F}(\mathbf{u}_n) \tag{6}$$

must hold. Then one can obtain from Eq. (5)

$$\frac{\partial}{\partial t}\int \mathbf{u}\, dv+\int T^{-1}\mathbf{F}(\mathbf{u}_n)\, ds=0. \tag{7}$$

Introducing new dependent variables $\mathbf{u}_1=(\rho, m_x, m_y, m_z, B_{1x}, B_{1y}, B_{1z}, U_1)^{\mathrm{T}}=(\rho, m_x, m_y, m_z, B_x-B_{0x}, B_y-B_{0y}, B_z-B_{0z}, U-(\mathbf{B}_1\cdot\mathbf{B}_0)/\beta-B_0{}^2/(2\beta))^{\mathrm{T}}$ with the conditions $\partial \mathbf{B}_0/\partial t=\mathrm{rot}\,\mathbf{B}_0=\mathrm{div}\,\mathbf{B}_0=0$, then the equation for $\mathbf{u}_1$ can be written in the conservation-law form as

$$\frac{\partial}{\partial t}\int \mathbf{u}_1\, dv+\int T^{-1}\bar{\mathbf{F}}(\mathbf{u}_{1n}, \mathbf{B}_{0n})\, ds=0, \tag{8}$$

with $\mathbf{u}_{1n}=T\mathbf{u}_1$, $\mathbf{m}_n=T_1\mathbf{m}=(m_n, m_{t1}, m_{t2})^{\mathrm{T}}$, $\mathbf{B}_n=T_1\mathbf{B}=(B_n, B_{t1}, B_{t2})^{\mathrm{T}}$, $\mathbf{B}_{1n}=T_1\mathbf{B}=(B_{1n}, B_{1t1}, B_{1t2})^{\mathrm{T}}$, $\mathbf{B}_{0n}=T_1\mathbf{B}_0=(B_{0n}, B_{0t1}, B_{0t2})^{\mathrm{T}}$, and

$$\bar{\mathbf{F}}=\begin{vmatrix} m_n \\ P+\dfrac{m_n m_n}{\rho}+\dfrac{B^2}{2\beta}-\dfrac{1}{\beta}B_nB_n-\dfrac{B_0{}^2}{2\beta}+\dfrac{1}{\beta}B_{0n}B_{0n} \\ \dfrac{m_{t1}m_n}{\rho}-\dfrac{1}{\beta}B_{t1}B_n+\dfrac{1}{\beta}B_{0t1}B_{0n} \\ \dfrac{m_{t2}m_n}{\rho}-\dfrac{1}{\beta}B_{t2}B_n+\dfrac{1}{\beta}B_{0t2}B_{0n} \\ 0 \\ \dfrac{m_n}{\rho}B_{t1}-\dfrac{m_{t1}}{\rho}B_n \\ \dfrac{m_n}{\rho}B_{t2}-\dfrac{m_{t2}}{\rho}B_n \\ \dfrac{m_n}{\rho}\left(U_1+\dfrac{B_1{}^2}{2\beta}+P\right)-\dfrac{B_{1n}}{\beta} \\ \quad\times\left(\dfrac{m_n}{\rho}B_{1n}+\dfrac{m_{t1}}{\rho}B_{1t1}+\dfrac{m_{t2}}{\rho}B_{1t2}\right) \\ \quad+\dfrac{B_{1t1}}{\beta}\left(\dfrac{m_n}{\rho}B_{0t1}-\dfrac{m_{t1}}{\rho}B_{0n}\right) \\ \quad+\dfrac{B_{1t2}}{\beta}\left(\dfrac{m_n}{\rho}B_{0t2}-\dfrac{m_{t2}}{\rho}B_{0n}\right) \end{vmatrix}. \tag{9}$$

In expression (9), the $\mathbf{B}_0$ terms are added to the second, third, and fourth components of $\bar{\mathbf{F}}$, considering $\mathrm{rot}\,\mathbf{B}_0\times\mathbf{B}_0=0$. Analytically, these terms are equal to zero. However, they are not zero numerically. For the derivation of the last component of F, the relation $\mathbf{m}\times\mathbf{B}\cdot\mathrm{rot}\,\mathbf{B}_0=0$ is applied. The first-order energy density U_1, density ρ, momentum $\mathbf{m}$, and first-order magnetic field $\mathbf{B}_1$ are related to pressure P by the equation

$$P=(\gamma-1)\left(U_1-\frac{m^2}{2\rho}-\frac{B_1{}^2}{2\beta}\right). \tag{10}$$

In these equations, the constants are β and γ, with $\beta=\mu\rho_0RT_0/B_{00}{}^2$, $\gamma=$ the polytropic index, $\mu=$ the magnetic permeability, $R=$ the gas constant, $\rho_0=$ the normalization density, $B_{00}=$ the normalization field, and

T_0 = the normalization temperature. Momentum $\mathbf{m}$ is normalized by $\rho_0(RT_0)^{1/2}$ and time t is normalized by $L_0/(RT_0)^{1/2}$, with L_0 = normalization length.

3. NUMERICAL METHOD

From Eq. (8), a discrete formula of MHD equations in the FVM style is written for the grid point i in the form

$$\frac{\partial}{\partial t}\mathbf{u}_{1i}V_i+\sum_j T^{-1}{}_{ij}\underline{\mathbf{F}}_{ij}(\mathbf{u}_{1ni'}, \mathbf{u}_{1ni}, \mathbf{u}_{tnj}, \mathbf{u}_{inj'}, \mathbf{B}_{0nij})\,S_{ij}=0, \tag{11}$$

where j denotes the grid points neighbouring the grid point i, V_i denotes the volume of the control volume cell which includes the grid point i, T_{ij} is the rotation matrix at the interfacing surface between i and j, S_{ij} is the surface area of the i and j interface, $\mathbf{u}_{1ni'}$, $\mathbf{u}_{1ni}$, $\mathbf{u}_{1nj}$, and $\mathbf{u}_{1nj'}$ are $\mathbf{u}_{1i'}$, $\mathbf{u}_{1i}$, $\mathbf{u}_{1j}$, and $\mathbf{u}_{1j'}$ rotated by T_{ij}, and $\mathbf{B}_{0nij}$ is $\mathbf{B}_{0n}$ at the i and j interface. In the first-order case, the upwind numerical flux $\underline{\mathbf{F}}_{ij}$ for (11) is

$$\underline{\mathbf{F}}_{ij}=\tfrac{1}{2}\{\bar{\mathbf{F}}(\mathbf{u}_{1nj}, \mathbf{B}_{0nij})+\bar{\mathbf{F}}(\mathbf{u}_{1ni}, \mathbf{B}_{0nij}) - R_{ij}\,|A_{ij}|\,R_{ij}{}^{-1}(\mathbf{u}_{1nj}-\mathbf{u}_{1ni})\}, \tag{12}$$

Here A_{ij}, the flux Jacobian matrix of $\bar{\mathbf{F}}$ at the i and j interface, is diagonalized for calculation of the mode synthesis matrix R_{ij} and the eigenvalue matrix Λ_{ij} from the relations

$$A_{ij}R_{ij}=R_{ij}\Lambda_{ij}, \tag{13a}$$

$$A_{ij}=\frac{\partial\bar{\mathbf{F}}}{\partial\mathbf{u}_{1n}}(\mathbf{u}_{1nij}, \mathbf{B}_{0nij}). \tag{13b}$$

As seen from Eq. (13a), the mode synthesis matrix consists of the right eigenvectors of the flux Jacobian matrix $\mathbf{r}_{ijk}$, and the diagonal matrix Λ_{ij} consists of eigenvalues λ_{ijk}, $k=1\sim 8$. Without suffix ij, the eigenvalues λ_k are written through $\mathbf{u}_n$ as [10]

$$\lambda_1=m'_n, \tag{14a}$$

$$\lambda_{2,3}=m'_n\pm|B'_n|, \tag{14b}$$

$$\lambda_{4,5}=m'_n\pm V_f, \tag{14c}$$

$$\lambda_{6,7}=m'_n\pm V_s, \tag{14d}$$

$$\lambda_8=0, \tag{14e}$$

where

$$V_f{}^2,\ V_s{}^2=\tfrac{1}{2}[C_0+B'^2\pm\{(C_0+B'^2)^2-4C_0B'_n{}^2\}^{1/2}], \tag{15a}$$

$$C_0=\gamma p/\rho, \tag{15b}$$

with the notation $\mathbf{u}'_n=(\rho,\ m'_n,\ m'_{t1},\ m'_{t2},\ B'_n,\ B'_{t1},\ B'_{t2},\ U)^{\mathrm{T}}=(\rho,\ m_n/\rho,\ m_{t1}/\rho,\ m_{t2}/\rho,\ B_n/\sqrt{\beta\rho},\ B_{t1}/\sqrt{\beta\rho},\ B_{t2}/\sqrt{\beta\rho},\ U)^{\mathrm{T}}$. Here, variables with ′ have a dimension of velocity. In the expression of eigenvalues, $\sqrt{C_0}$, $|B'_n|$, V_f, and V_s correspond to sound, Alfven, fast, and slow velocities, respectively. Calculations of eigen vectors must be done with special care, avoiding the degeneration of the eigen vectors when the wave propagation becomes perpendicular or parallel to the magnetic field. Without ij, the right eigen vectors $\mathbf{r}_k$ which correspond to λ_k are:

$$\mathbf{r}_1=\begin{vmatrix}1\\ m'_n\\ m'_{t1}\\ m'_{t2}\\ 0\\ 0\\ 0\\ 0.5\cdot m'^2\end{vmatrix}, \tag{16a}$$

$$\mathbf{r}_{2,3}=\begin{vmatrix}0\\ 0\\ \mp B''_{t2}\cdot\mathrm{sgn}(B'_n)\\ \pm B''_{t1}\cdot\mathrm{sgn}(B'_n)\\ 0\\ B''_{t2}\sqrt{\beta/\rho}\\ -B''_{t1}\sqrt{\beta/\rho}\\ \mp(B''_{t2}m'_{t1}-B''_{t1}m'_{t2})\cdot\mathrm{sgn}(B'_n)\\ \quad+(B''_{t2}B_1'{}_{t1}-B''_{t1}B_1'{}_{t2})\end{vmatrix}, \tag{16b}$$

$$\mathbf{r}_{4,5}=\begin{vmatrix}a_f\\ a_f(m'_n\pm V_f)\\ a_fm'_{t1}\mp a_sB''_{t1}V_fB'_n\\ a_fm'_{t2}\mp a_sB''_{t2}V_fB'_n\\ 0\\ a_sB''_{t1}V_f{}^2\sqrt{\beta/\rho}\\ a_sB''_{t2}V_f{}^2\sqrt{\beta/\rho}\\ a_f\cdot 0.5\cdot m'^2+a_fV_f{}^2/(\gamma-1)\pm a_fV_fm'_n\\ \quad\mp a_sV_f(B''_{t1}m'_{t1}+B''_{t2}m'_{t2})\cdot B'_n\\ \quad+a_f(-1)/(\gamma-1)\cdot(v_f{}^2-C_0)\\ \quad+a_f\cdot(v_f{}^2-C_0)(B''_{t1}B_1''_{t1}\\ \quad+B''_{t2}B_1''_{t2})/(B''_{t1}{}^2+B''_{t2}{}^2)\end{vmatrix}, \tag{16c}$$

$$\mathbf{r}_{6,7}=\begin{vmatrix}a_s\\ a_s(m'_n\pm V_s)\\ a_sm'_{t1}\pm a_fB''_{t1}\sqrt{C_0}/V_f\cdot\mathrm{sgn}(B'_n)\\ a_sm'_{t2}\pm a_fB''_{t2}\sqrt{C_0}/V_f\cdot\mathrm{sgn}(B'_n)\\ 0\\ -a_fB''_{t1}\sqrt{\beta/\rho}\cdot C_0/V_f{}^2\\ -a_fB''_{t2}\sqrt{\beta/\rho}\cdot C_0/V_f{}^2\\ a_s\cdot 0.5\cdot m'^2+a_sV_s{}^2/(\gamma-1)\pm a_sV_sm'_n\\ \quad\pm a_f(B''_{t1}m'_{t1}+B''_{t2}m'_{t2})\\ \quad\times\sqrt{C_0}/V_f\cdot\mathrm{sgn}(B'_n)+a_s(-1)/(\gamma-1)\cdot(v_s{}^2-C_0)\\ \quad+a_s\cdot(v_s{}^2-C_0)(B''_{t1}B_1''_{t1}\\ \quad+B''_{t2}B_1''_{t2})/(B''_{t1}{}^2+B''_{t2}{}^2)\end{vmatrix}, \tag{16d}$$

where

$$B''_{t1} = (B'_{t1} + \varepsilon)/(B'^2_{t1} + B'^2_{t2} + 2\varepsilon^2)^{1/2}, \quad (17a)$$

$$B_1''_{t1} = (B_1'_{t1} + \varepsilon)/(B'^2_{t1} + B'^2_{t2} + 2\varepsilon^2)^{1/2}, \quad (17b)$$

$$B''_{t2} = (B'_{t2} + \varepsilon)/(B'^2_{t1} + B'^2_{t2} + 2\varepsilon^2)^{1/2}, \quad (17c)$$

$$B_1''_{t2} = (B_1'_{t2} + \varepsilon)/(B'^2_{t1} + B'^2_{t2} + 2\varepsilon^2)^{1/2}, \quad (17d)$$

$$\mathbf{B}_1'_n = \mathbf{B}_{1n}/\sqrt{\beta\rho}, \quad (17e)$$

$$a_f = (V_f^2 - B'^2_n)^{1/2}/(V_f^2 - V_s^2)^{1/2}, \quad (17f)$$

$$a_s = (V_f^2 - C_0)^{1/2}/(V_f^2 - V_s^2)^{1/2}\, V_f, \quad (17g)$$

and ε is a small number. Comparing Eqs. (16a)–(16d) with the case of $\mathbf{B}_0 = 0$, given by Brio and Wu [10], only the last components of $\mathbf{r}_2 \sim \mathbf{r}_7$ are different. They are written through not only $\mathbf{B}_n = \mathbf{B}_{0n} + \mathbf{B}_{1n}$ but also $\mathbf{B}_{1n}$. For $\mathbf{r}_8$, a unit vector is used with a small value for λ_8. For the evaluation of A_{ij}, some averaging procedure must be introduced to determine $\mathbf{u}_{1nij}$, the symmetric average of $\mathbf{u}_{1ni}$ and $\mathbf{u}_{1nj}$. Theoretically, the optimum choice for $\mathbf{u}_{1nij}$ is the Roe average of $\mathbf{u}_{1ni}$ and $\mathbf{u}_{1nj}$. However, such an averaging procedure is not known for MHD equations. Therefore, a simple averaging procedure is employed approximately, although this procedure does not satisfy the first condition for Roe's matrix.

To obtain a higher order of accuracy, the MUSCL approach is used, changing i and j to L and R, suffixes which indicate variables just on the negative and positive sides of the interface, in Eq. (12). Then the numerical flux is defined by the relation

$$\underline{F}_{ij} = \tfrac{1}{2}\{\bar{\mathbf{F}}(\mathbf{u}_{1nR}, \mathbf{B}_{0nij}) + \bar{\mathbf{F}}(\mathbf{u}_{1nL}, \mathbf{B}_{0nij}) - R_{RL}\,|\Lambda_{RL}|\,R_{RL}^{-1}(\mathbf{u}_{1nR} - \mathbf{u}_{1nL})\}, \quad (18)$$

with

$$A_{RL}R_{RL} = R_{RL}\Lambda_{RL}, \quad (19a)$$

$$\mathbf{u}_{1nL} = \mathbf{u}_{1ni} + s_i\{(1 - \tfrac{1}{3}s_i)(\mathbf{u}_{1ni} - \mathbf{u}_{1ni'}) + (1 + \tfrac{1}{3}s_i)(\mathbf{u}_{1nj} - \mathbf{u}_{1ni})\}/4, \quad (19b)$$

$$\mathbf{u}_{1nR} = \mathbf{u}_{1nj} - s_j\{(1 - \tfrac{1}{3}s_j)(\mathbf{u}_{1nj'} - \mathbf{u}_{1nj}) + (1 + \tfrac{1}{3}s_j)(\mathbf{u}_{1nj} - \mathbf{u}_{1ni})\}/4, \quad (19c)$$

where the diagonal matrixes s_i and s_j consist of the so-called Van Leer's differentiable limiter. The kth components of s_i and s_j are calculated from the kth components of $\mathbf{u}_{1n}$. Without suffix k, they are written as

$$s_i = \frac{2(u_{1nj} - u_{1ni})(u_{1ni} - u_{1ni'}) + \varepsilon}{(u_{1nj} - u_{1ni})^2 + (u_{1ni} - u_{1ni'})^2 + \varepsilon}, \quad (20a)$$

$$s_j = \frac{2(u_{1nj'} - u_{1nj})(u_{1nj} - u_{1ni}) + \varepsilon}{(u_{1nj'} - u_{1nj})^2 + (u_{1nj} - u_{1ni})^2 + \varepsilon}. \quad (20b)$$

In the MUSCL interpolation procedure given by Eqs. (19b) and (19c), a fixed stencil is used. Interpolation points i' and j' are obtained by extending the line which connects grid points i and j to the neighbouring surface of control volumes.

A serious problem in numerical MHD simulation is the violation of the div $\mathbf{B} = 0$ condition. Not only numerical roundoff errors but also the use of upwind fluxes and a non-cartesian grid system make it hard to fulfill the div $\mathbf{B} = 0$ condition automatically as Caramana [16] did. In the present calculation, an extra equation is added for the elimination of artificial magnetic monopoles. According to Schmidt-Voigt [3], first-order magnetic field $\mathbf{B}_1$ is replaced at every several time steps, by a new field $\mathbf{B}_{1c}$ given as

$$\mathbf{B}_{1c} = \mathbf{B}_1 + \text{grad}\ \phi, \quad (21a)$$

$$\nabla^2\phi = -\text{div}\ \mathbf{B}_1. \quad (21b)$$

The Poisson equation (21b) for the divergence-cleaning potential ϕ is written in FVM form as

$$\sum_j \frac{1}{2}\left(\frac{\mathbf{n}_{ij}\cdot(\mathbf{r}_j - \mathbf{r}_{i'})(\phi_j - \phi_{i'})}{(\mathbf{r}_j - \mathbf{r}_{i'})^2} + \frac{\mathbf{n}_{ij}\cdot(\mathbf{r}_{j'} - \mathbf{r}_i)(\phi_{j'} - \phi_i)}{(\mathbf{r}_{j'} - \mathbf{r}_i)^2}\right) S_{ij} = -\sum_j B_{1nij} S_{ij}, \quad (22)$$

where $\mathbf{r}_{j'}$, $\mathbf{r}_j$, $\mathbf{r}_i$, and $\mathbf{r}_{i'}$ are the position vectors of the j', j, i, and i' points, $\mathbf{n}_{ij}$ is a unit vector normal to the interfacing surface between control volumes i and j. To solve Eq. (22), the conjugate residual (CR) method is applied.

There may be a case in which the divergence-cleaning procedure given by (21a) and (21b) spoils the TVD property of the scheme. However, it will be shown from a numerical example in the following sections that sharp shock-capturing properties are retained despite the use of this divergence-cleaning procedure.

4. A TEST PROBLEM

In this section, a test problem is presented to show the efficiency of above-mentioned scheme. As a numerical example, we treat a system which consists of a dipole magnetic field $\mathbf{B}_d$ placed at $x = y = z = 0$ and an external incoming MHD flow.

The grid system for the numerical calculation is generated from the spherical coordinate (r, θ, ϕ), with the number of grids to be $(36 \times 40 \times 48)$ in the (r, θ, ϕ) directions. By this grid system, the region of $1 < r < 10$, $-\pi/2 < \theta < \pi/2$, and $0 < \phi < 2\pi$ is covered adopting uniform grid point spacings for θ and ϕ, and non-uniform grid point spacings for r. Then

r, θ, and ϕ coordinates of grid points are given through suffixes i, j, and k by

$$r_{ijk} = 1 + 0.1(i-1) + 5.5(i-1)^{2.5}/35^{2.5}, \tag{23a}$$

$$\theta_{ijk} = (j-1)\,\pi/39 - \pi/2, \tag{23b}$$

$$\phi_{ijk} = (k-1)\,\pi/24, \tag{23c}$$

with $1 \leqq i \leqq 36$, $1 \leqq j \leqq 40$, and $1 \leqq k \leqq 48$. The grid spacings in the r direction vary from 0.1 at $r = 1$ to about 0.5 near the outer boundary, considering the fact that small-scale flow structures appear near the root of a dipole field. Because the resulting grid system has nesting grid points at $\theta = \pm\pi/2$, it cannot be treated as a structured grid system. The x, y, and z axes are chosen to the direction of $\phi = \pi$, $\phi = 3\pi/2$, and $\theta = \pi/2$, respectively. In this paper we want to call the xy plane as the equatorial plane, due to the analogy with planetary coordinates in the solar terrestrial system. Similarly, we call the direction of the y axis and the z axis the dusk side and the north pole. Then, the flow velocity at the upstream region is assumed to be poining toward the $-x$ direction, including a magnetic field which is pointing toward the $-y$ direction. The potential field $\mathbf{B}_0$ is given from $\mathbf{B}_d = (0, 0, -100)^{\mathrm{T}}$ as

$$\mathbf{B}_0 = \frac{1}{r^3}\,(3\mathbf{n}_r(\mathbf{B}_d \cdot \mathbf{n}_r) - \mathbf{B}_d), \tag{24}$$

where $\mathbf{n}_r$ is a unit vector in the r direction.

The inner boundary conditions at $r = 1$ are given by

$$\rho = \rho_b \quad \text{for} \quad (\mathbf{m} \cdot \mathbf{n}_r) > 0, \tag{25a}$$

$$\partial\rho/\partial r = 0 \quad \text{for} \quad (\mathbf{m} \cdot \mathbf{n}_r) < 0, \tag{25b}$$

$$\partial(r^2(\mathbf{m} \cdot \mathbf{n}_b))/\partial r = 0, \tag{25c}$$

$$\mathbf{m} \times \mathbf{B}_0 = 0, \tag{25d}$$

$$(\mathbf{B}_1 \cdot \mathbf{n}_r) = 0, \tag{25e}$$

$$\partial(r(\mathbf{B}_1 - (\mathbf{B}_1 \cdot \mathbf{n}_r)\,\mathbf{n}_r))/\partial r = 0, \tag{25f}$$

$$U_1 = \frac{\rho T}{\gamma - 1} + \frac{m^2}{2\rho} + \frac{{B_1}^2}{2\beta}, \tag{25g}$$

with $T = T_b$ for $(\mathbf{m} \cdot \mathbf{n}_r) > 0$ and $\partial T/\partial r = 0$ for $(\mathbf{m} \cdot \mathbf{n}_r) < 0$, where ρ_b and T_b are the density and temperature of the plasma flowing to the calculating region from the inner boundary. In the present calculation, $\rho_b = 0.1$ and $T_b = 1$ are adopted; $\mathbf{n}_b$ is a unit vector in the direction of magnetic field.

Outer boundary conditions at the upstream part of $r = 10$ and $\pi/2 < \phi < 3\pi/2$ are

$$\rho = 1, \tag{26a}$$

$$m_x = -2.5, \qquad m_y = m_z = 0, \tag{26b}$$

$$B_x = B_z = 0, \qquad B_y = -0.2, \tag{26c}$$

$$U_1 = \frac{\rho T_b}{\gamma - 1} + \frac{m^2}{2\rho} + \frac{{B_1}^2}{2\beta}, \tag{26d}$$

where T_b is the upstream flow temperature measured by T_0. The outer boundary conditions at the downstream part of $r = 10$ and $-\pi/2 < \phi < \pi/2$ are given for all dependent variables by $\partial/\partial x = 0$.

The initial conditions for density and temperature are $\rho = 1$ and $T = T_b = 0.8$ every where. Spatial distributions of $\mathbf{m}$ for the initial states are given for $r_1 = 3 < r$ from the potential flow past a sphere,

$$\mathbf{m} = \mathbf{m}_b - \frac{1}{2(r/r_1)^3}\,(3\mathbf{n}_r(\mathbf{m}_b \cdot \mathbf{n}_r) - \mathbf{m}_b), \tag{27}$$

with $\mathbf{m}_b = (-2.5, 0, 0)^{\mathrm{T}}$. Similarly, $\mathbf{B}_1$ for the initial state is given by

$$\mathbf{B}_1 = \mathbf{B}_b - \frac{1}{2(r/r_1)^3}\,(3\mathbf{n}_r(\mathbf{B}_b \cdot \mathbf{n}_r) - \mathbf{B}_b) - \frac{1}{r^3}\,(3\mathbf{n}_r(\mathbf{B}_d \cdot \mathbf{n}_r) - \mathbf{B}_d) + \frac{2{r_1}^3\mathbf{B}_d}{{r_2}^6}, \tag{28}$$

for $r_2 = 9 < r$ with $\mathbf{B}_b = (0, -0.2, 0)^{\mathrm{T}} - 2{r_1}^3\mathbf{B}_d/{r_2}^6$, and

$$\mathbf{B}_1 = \mathbf{B}_b - \frac{1}{2(r/r_1)^3}\,(3\mathbf{n}_r(\mathbf{B}_b \cdot \mathbf{n}_r) - \mathbf{B}_b) - \frac{2\mathbf{B}_d}{{r_2}^3} + \frac{{r_1}^3}{r^3{r_2}^3}\,(3\mathbf{n}_r(\mathbf{B}_d \cdot \mathbf{n}_r) - \mathbf{B}_d), \tag{29}$$

for $r_1 < r < r_2$. The initial condition for $\mathbf{B}_1$ thus calculated can roughly satisfy the outer boundary conditions while it retains the div $\mathbf{B}_1 = 0$ condition.

In the present problem, some eigenvalues vary over a wide range in the calculation region while some eigenvalues are almost constant. As a result, the ratio of maximum λ_{ijk} to minimum λ_{ijk} becomes very large near the inner boundary. Therefore, the values of $|\lambda_{ijk}|$ are modified in Eq. (18) as

$$|\lambda_{ijk}| = \max(|\lambda_{ijk}|,\, \delta \times \max(k)\,|\lambda_{ijk}|), \tag{30}$$

where δ is a small constant.

An explicit method is selected as the time integration method. In this method, the CFL number must be less than 1.0. Therefore time step Δt is chosen to be

$$\Delta t = 0.9/\max(ijk)\left(\frac{S_{ij}}{V_i}\,\lambda_{ijk}\right). \tag{31}$$

The test problem presented in this section can be looked upon as an idealized model of solar–wind interaction with a

planet having a dipole-like magnetic field. In the case of the Earth, the problem is properly scaled by selecting $L_0 = 3R_e$, with R_e the radius of the Earth. Simulating the situation of the solar wind, $\beta = 5$ is adopted to give a high β solar wind. As for the ratio of the specific heats, $\gamma = 1.30$ is selected for the simulation of solar wind conditions. Considering values of γ, T, ρ, and m_x, the Mach number of incoming flow becomes about 2.5. On the other hand, the magnitude of the dipole field is set as $|B_0| = 100$ at $r = 1$ and $\theta = 0$. Thus, a low-β condition is realized at the inner boundary, while a high-β condition is retained at the outer boundary. In the present calculation, parameters selected are not exactly the same as the case of the solar–wind interaction with the Earth. However, the present parameters reproduce the most important situation of the problem that an essence of the problem is the interaction of high-β supersonic plasma flow with the region of strong magnetic field including magnetized low-β plasma. In the present situation, the inner boundary corresponds to the ionosphere, where the plasma velocity perpendicular to the ambient magnetic field must be decided from the FAI flowing into the ionosphere and the ionospheric conductivity as

$$\nabla \cdot \sigma \nabla \phi_I = (\mathrm{rot}\, \mathbf{B}_1 \cdot \mathbf{n}_r)_{r=1}, \tag{32a}$$

$$\mathbf{m} - (\mathbf{m} \cdot \mathbf{n}_b)\, \mathbf{n}_b = \rho \frac{\nabla \phi_I \times \mathbf{B}_0}{{B_0}^2}, \tag{32b}$$

where σ and ϕ_I are the ionospheric conductivity and potential. In order to sufficiently analyze Eq. (32a) in the ionosphere, there occurs a requirement that a sufficient number of grid points must be allocated on the inner boundary. From this point of view, the inner boundary condition (25d) corresponds to the case of infinite conductivity in the ionosphere. The process of the solar wind–magnetosphere–ionosphere coupling with these boundary conditions cannot be simulated effectively, without the use of unstructured grid systems.

5. RESULTS OF CALCULATION

Figure 1 plots a 3D configuration of the calculated magnetic field $\mathbf{B} = \mathbf{B}_0 + \mathbf{B}_1$. Here, magnetic fields that thread the inner boundary are shown, with the left of the figure to the downstream ($-x$ or anti-sunward) direction. The supersonic plasma flow that impinges on the dipole field exerts dynamic pressure on the magnetic field. As a result, the magnetic field is compressed on the upstream (x or sunward) side and blown down on the opposite side into a tail-like configuration. Thus, the intrinsic magnetic field develops into the magnetosphere, as can be observed in this figure. The outer boundary of the confined magnetic field constructing the magnetosphere is called the magnetopause.

The upper and lower halves of Fig. 2 exhibit the pressure

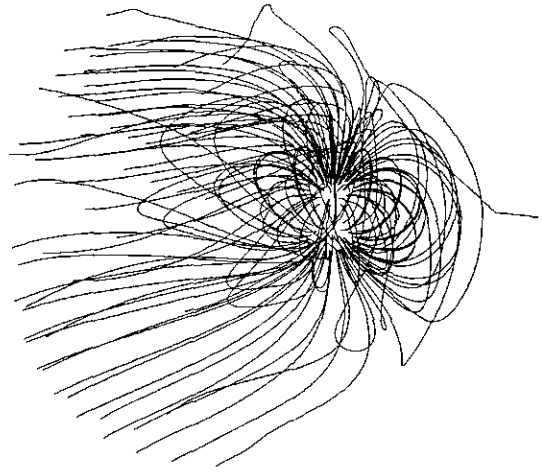

FIG. 1. 3D plot of magnetic field lines which originate from the inner boundary. The x-axis (sunward direction) is toward the right and z-axis (northward direction) is toward the top.

distributions in the noon–midnight meridian (xz) plane and in the equatorial (xy) plane. In this figure, the formation of a bow shock can be observed in the upstream region, as a sharp increase of P to the downstream direction. There appears a high-pressure region between the bow shock and the magnetopause. This region surrounding the magnetosphere is filled with shocked flowing plasma and called the magnetosheath. In the meridian plane, a narrow region which includes high-pressure plasma extends from the magnetosheath to the inner boundary. This narrow

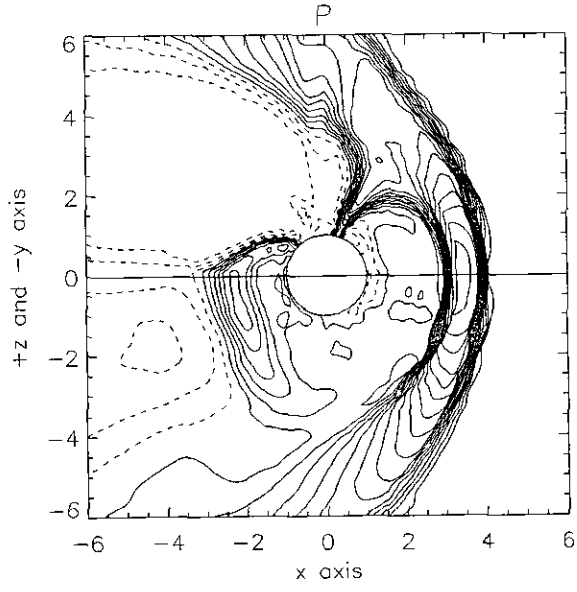

FIG. 2. Distribution of the pressure P in the noon–midnight meridian (xz) and the equatorial (xy) planes. Contours are shown by solid lines for the pressure levels greater than those in the incoming flow, and by dotted lines for the smaller levels. The difference between contours $\Delta P = 0.22$.

region called the dayside cusp is exhibited very precisely in the present calculation. Such a clear representation of the dayside cusp had never been obtained in earlier works based on the structured grid systems [2, 5]. For instance, Watanabe and Sato [5] gave a less obvious cusp structure, although the total number of grid points used by them was about 40 times larger than the present calculation.

Another high-pressure region behind the planet in the downstream side is called the nightside cusp. Following the nightside cusp, a relatively high-density region spreads widely in the downstream equatorial plane. This region called the plasmasheet carries field-reversing sheet current and divides the northern and southern low-pressure regions in the tail part of the magnetosphere. Thus, the plasmasheet is compressed in the meridional plane. The high-pressure region which extends from the nightside cusp toward the planet along the magnetic field reaches as far as the inner boundary. In the equatorial plane, the ring current which surrounds the near planet region is formed as an extension of the high-pressure region from the night-side cusp. These structures in the inner magnetosphere can be calculated precisely, because the unstructured grid system enables us to allocate sufficient grid points near the inner boundary without a severe increase in the total number of grid points.

The low-pressure region north and south of the plasma sheet (around $1 < z < 5$ and $x < -1$ in Fig. 2) is called the lobe. Near the inner boundary, the density distribution in the lobe is related to the inner boundary conditions (25a) and (25g). At the root of the magnetic field line which connects the inner boundary with the lobe, the flow velocity on the inner boundary becomes outward, due to the evacuation effect. In this case, it is necessary to fix more dependent variables at the inner boundary, compared with the case of inward flow. Thus, the density and pressure in the lobe depend on the capacity of the ionosphere as an emitter of plasma.

Figure 3 shows the distribution of the anti-sunward velocity $-V_x = -m_x/\rho$ in the dawn–dusk meridian (yz) plane. In the region outside the magnetopause, high-speed flows dominate toward the anti-sunward direction. Near the inner boundary, on the other hand, slower anti-sunward ($-x$) convections dominate in the polar region, while sunward ($+x$) return flows are seen around the ring-current region. The anti-sunward and sunward flows extend to the inner boundary along the magnetic field. These plasma motions in the magnetosphere correspond to the magnetospheric convection induced by the solar wind–magnetosphere interaction. In the present calculation, extensions of the magnetospheric convection to the ionospheric region are represented very clearly.

In the ideal case, the boundary condition (25d) will suppress the plasma convection in the magnetosphere. However, magnetospheric plasma convection can be induced because the numerical diffusion cannot be exactly

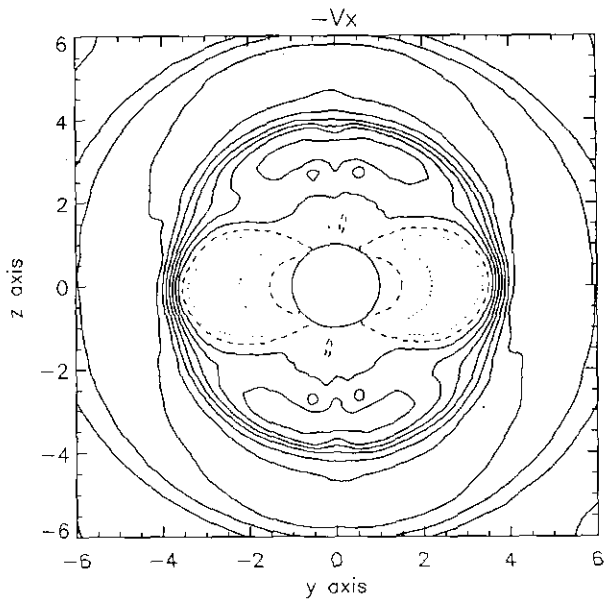

FIG. 3. Distribution of anti-sunward velocity $-V_x = -m_x/\rho$ in the dawn–dusk meridian (yz) plane. Solid, dashed, and dotted lines indicate plus (anti-sunward), zero, and minus (sunward) contours, respectively. The difference between contours $\Delta V_x = 0.22$.

zero. In a real situation, this diffusion effect is offered by the atmospheric drag due to the collisional interaction of plasma with the neural atmosphere around the planet. On the inner boundary, the region of anti-sunward flow and the boundary between the anti-sunward and sunward flows correspond to the polar cap and the auroral oval, respectively.

Figure 4 shows the distributions of plasma pressure P, the east–west component of magnetic field B_y, north–south component of magnetic field B_z and the $-x$ component of velocity $-V_x$, along the x axis for the sun–earth line. The vertical scale for B_z is $\frac{1}{10}$ of other parameters. In this figure, the positions of grid points are shown by marks on the curves. The pressure and B_y suddenly increase at the bow

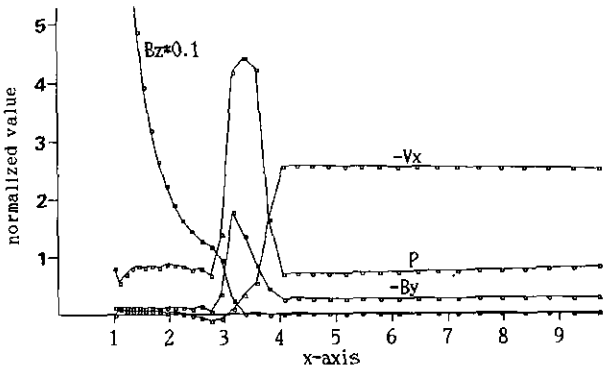

FIG. 4. Distributions of P, $-V_x$, $-B_y$, and $0.1 \times B_z$ along the sun–planet line. Note that the vertical scale for B_z is $\frac{1}{10}$ the other parameters.

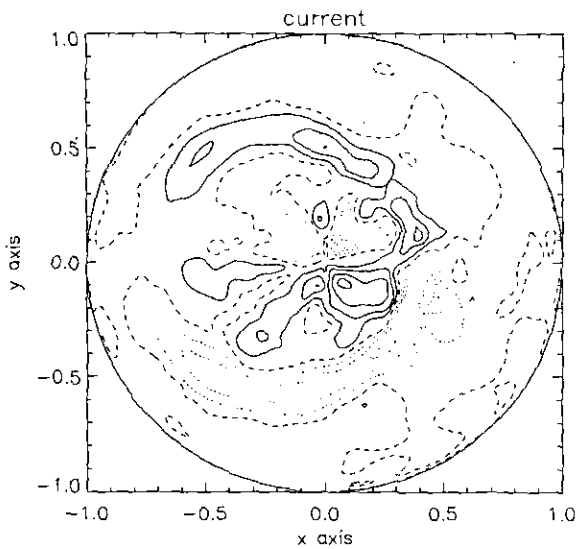

FIG. 5. Distribution of field-aligned current (FAI) flowing into and out of the inner boundary. This figure shows the top view of the sphere which forms the inner boundary. Solid, dashed, and dotted lines show contours for outward, zero, and inward currents, respectively.

shock, while $-V_x$ decreases there. This is the signature of a fast shock. Behind the bow shock, P decreases at the magnetopause, forming a tangential discontinuity. Structures of the bow shock and magnetopause are resolved by few grid points. From these results, it is proved that the TVD scheme enables an effective calculation of the MHD equations with sharp shock capturings.

In the present calculation, sufficient grid points are allocated on the inner boundary. Therefore, direct calculation of FAI becomes possible from $\mathbf{B}_1$ on the inner boundary. Figure 5 shows the top view of the spherical surface at $r = 1$, on which the distribution of FAI flowing into or out of the inner boundary is drawn. The region of strong FAI composed of dawn $(-y)$ downward and dusk $(+y)$ upward currents forms a partial ring, which is called region-1 current. Equator-ward of the region-1 current, very weak current systems are seen on the dawn and dusk sides. These current systems are connected to the ring-current region in the magnetosphere and are called the region-2 current. Pole-ward of the region-1 current, a current pair is seen around the foot of the dayside cusp shown in Fig. 2. This current pair is called the region-0 current. Thus, the present calculation can represent current systems very precisely. The feeding of FAI to the ionosphere is an important result of the solar wind–magnetosphere–ionosphere coupling. Here we can conclude that the coupling process between three different regions namely the solar wind, the magnetosphere, and the ionosphere, is simulated successfully, despite the different characteristics of three regions and the existence of a background inhomogeneous potential field.

6. SUMMARY

In this paper, a 3D MHD simulation scheme is developed for inhomogeneous systems, including a strong potential field. The algorithm is (1) written in a formula which avoids direct inclusions of background potential magnetic field as dependent variables, (2) applicable on an unstructured grid system due to the formulation by the finite volume method, (3) capable of calculations with high resolution and efficient shock capturings through the use of a MUSCL-type TVD scheme, and (4) completed with the support of a divergence-cleaning procedure. From a test problem, in which high-β supersonic plasma flow interacts with the region of strong magnetic field including magnetized low-β plasma, an ability of efficient calculations and nonoscillatory behavior of the scheme are demonstrated for the problem of inhomogeneous MHD calculations.

REFERENCES

1. M. Ashour-Abdalla and D. A. Dutton, *Space Plasma Simulations* (Reidel, Hingham, MA, 1985).
2. T. Ogino, *J. Geophys. Res.* **91**, 6791 (1986).
3. M. Schmidt-Voigt, *Astron. Astrophys.* **210**, 433 (1989).
4. Y. Q. Hu, *J. Comput. Phys.* **84**, 441 (1989).
5. K. Watanabe and T. Sato, *J. Geophys. Res.* **95**, 75 (1990).
6. H. C. Yee, NASA Technical Memorandum 89464, 1987 (unpublished).
7. M. M. Rai and S. R. Chakravarthy, *AIAA J.* **24**, 735 (1986).
8. A. Harten, *J. Comput. Phys.* **83**, 148 (1989).
9. H. C. Yee, G. H. Klopfer, and J. L. Montagne, *J. Comput. Phys.* **88**, 31 (1990).
10. M. Brio and C. C. Wu, *J. Comput. Phys.* **75**, 400 (1988).
11. T. Tanaka, *Comput. Fluid Dynam. J.* **1**, 14 (1992).
12. M. Vinokur, *J. Comput. Phys.* **81**, 1 (1989).
13. S.-I. Akasofu, "What Is a Magnetospheric Substorm?," in *Dynamics of the Magnetosphere*, edited by S.-I. Akasofu, (Reidel, Hingham, MA, 1980), p. 447.
14. P. Stern, *J. Geophys. Res.* **95**, 12057 (1990).
15. J. R. Kan, L. Zhu, and S.-I. Akasofu, *J. Geophys. Res.* **93**, 5624 (1988).
16. E. J. Caramana, *J. Comput. Phys.* **82**, 492 (1989).